Available online at BCREC website: https://bcrec.id

Bulletin of Chemical Reaction Engineering & Catalysis, 18 (4) 2023, 648-658

Research Article

1D/2D Rod-sheet Shape Bi_2S_3 Photocatalyst for Photocatalytic Reduction Cr(VI) under Visible Light

Xinzhuo Wu[1,2], Shaojie Chen[2], Yinxing Jiang[2], Xinshan Zhao[1,2], Zhao Li[2], Yingmei Zhou[2], Jing Li[1,2,*]

[1]School of Chemistry and Environmental Science, Yili Normal University, 835000, Yining, China
[2]School of Materials and Chemical Engineering, Xuzhou University of Technology, 221018, Xuzhou, China

Received: 14th October 2023; Revised: 10th November 2023; Accepted: 11st November 2023
Available online: 15th November 2023; Published regularly: December 2023

Abstract

The crystal structure and morphology of photocatalysts play a crucial role in determining their photocatalytic performance. In this study, we synthesized and investigated 1D/2D Bi_2S_3 as a potential visible-light-activated photocatalyst for the reduction of aqueous Cr(VI). The 1D/2D Bi_2S_3 was synthesized using hydrothermal synthesis technique by heating $Bi_2(H_2O)_2(SO_4)_2(OH)_2$ precursor and sodium sulfide at 190 °C for 24 h, where the molar ratio of Bi to S elements in the reaction reagents was changed from 1:6 to 2:3. The structure, composition, and optoelectronic properties of the prepared Bi_2S_3 were characterized using X-ray diffraction, UV-vis diffuse reflectance spectra, field emission scanning electron microscopy, electrochemical impedance spectra, and transient photocurrent. It is shown that the prepared orthorhombic Bi_2S_3 has full-spectrum photoresponsivity. Bi_2S_3-B with 1D/2D heterogeneous structure exhibits the lowest charge carrier transport resistance, and its photocurrent intensity is nearly twice that of Bi_2S_3-C. It demonstrates the highest photocatalytic activity in visible-light photocatalytic reduction of aqueous Cr(VI), with a reduction rate of 54.5% after 140 minutes of light exposure. According to the bandgap of Bi_2S_3 and radical scavenger experiments, a reaction mechanism for the photocatalytic reduction of Cr(VI) by Bi_2S_3 was proposed. Furthermore, the results highlight the economic and environmentally friendly nature of the hydrothermal synthesis method using homemade precursors, which allows for the regulation of Bi_2S_3 morphology and the enhancement of its visible photocatalytic activity.

Keywords: Bi_2S_3; $Bi_2(H_2O)_2(SO_4)_2(OH)_2$ precursor; hydrothermal synthesis; Cr(VI) reduction; 1D/2D materials

How to Cite: Wu, X., Chen, S., Jiang, Y., Zhao, X., Li, Z., Zhou, Y., Li, J. (2023). 1D/2D Rod-sheet Shape Bi_2S_3 Photocatalyst for Photocatalytic Reduction Cr(VI) under Visible Light. *Bulletin of Chemical Reaction Engineering & Catalysis*, 18(4), 648-658 (doi: 10.9767/bcrec.20054)

Permalink/DOI: https://doi.org/10.9767/bcrec.20054

1. Introduction

Photocatalytic technology is a widely used advanced technology in the fields of environment and energy, known for its green, low-carbon, and sustainable characteristics [1–11]. The photocatalytic reaction usually includes several key steps as follows [2–7]: (1) photons with energy greater than the semiconductor forbidden band gap are required as an energy source; (2) Photocatalysts absorb the energy of incident photons and are excited to produce photogenerated carriers; (3) Separation and recombination of photogenerated e^-–h^+ pairs; and (4) Migration of photogenerated carriers to the photocatalyst surface for redox reactions.

The crystal structure and morphology of photocatalysts play a crucial role in determining their photocatalytic performance. One-dimensional (1D) nano photocatalytic materials, characterized by their unique nano range, accel-

* Corresponding Author.
Email: lijingxz111@163.com (J. Li)

erate photogenerated carriers migration and suppress the recombination of photogenerated e^-–h^+ pairs [1–10]. On the other hand, two-dimensional (2D) nanomaterials offer the advantages of large a specific surface area, numerous reactive sites, and shorter diffusion paths, which facilitate exciton dissociation and free charge transfer [4]. 1D/2D heterojunction photocatalysts combine the advantages of 1D rods and 2D nanosheets, effectively increasing the specific surface area, exposing more reactive surfaces, and increasing charge separation and transfer rate. This results in improved photocatalytic oxidation and reduction properties. Recently, the development of 1D/2D multiphase photocatalysts [4–13], such as $Bi_2O_2CO_3/Bi_2WO_6$ [4], $TiO_2/ZnIn_2S_4$ [5], CdS/WS_2 [6], α-Fe_2O_3/SnO_2 [7], Bi_2S_3/MoS_2 [11], Bi_2S_3/Ti_3C_2 [13], have shown promising applications in photocatalytic hydrogen production, environmental pollutant detection, wastewater pollutant degradation, and energy conversion [4–13].

The binary metal-sulfur compounds $A_2^{V}B_3^{VI}$ (A = As, Sb, Bi. B = S, Se, Te) have unique optical and electrical properties, making them widely used in energy conversion materials research [14]. Among these compounds, Bi_2S_3 is a semiconductor photocatalyst with a narrow bandgap (E_g = 1.3–1.7 eV) and broad spectral absorption properties. It has been proven to be an excellent material for photosensitizing and light-absorbing applications [14–18]. Bi_2S_3 can be used to construct heterojunction materials and is widely applied in renewable energy and environmental remediation [12,15–18]. Bi_2S_3 offers controllable morphology through valuable synthesis methods and synthesis conditions, enabling a variety of morphological structures including 1D and 2D materials.

Motaung *et al*. [14] prepared Bi_2S_3 nanoparticles using N-methyl-Nethanoldithiocarbamate complexes of Bi(III) as precursor and ethylene glycol solvent as solvent using microwave irradiation technique. Do *et al*. [19] prepared Bi_2S_3 nanowires with diameters of 60–80 nm and lengths of more than 1 µm using a simple hydrothermal synthesis technique and investigated the lattice dynamics and micro-Raman scattering of Bi_2S_3, as well as the photocatalytic treatment of hexavalent chromium-containing wastewater. Arumugam *et al*. [20] prepared Bi_2S_3 nanorods via the refluxing method using bismuth nitrate, thiourea, and cetyltrimethylammonium bromide as reactants, and the performance of Bi_2S_3 for photocatalytic degradation of methylene blue was investigated. The experimental results showed that reaction time and temperature were the important factors controlling the morphology of Bi_2S_3, and the high aspect ratio of the nanorods realized the optical blue shift phenomenon. Sasikala *et al*. [21] synthesized Bi_2S_3 nanowires and nanorods via microwave irradiation method using N,N-dimethylformamide, and ethylene glycol as solvents, respectively, and honeycomb shape Bi_2S_3 consisting of nanosheets in mixed solvents was obtained to have optimum photocatalytic degradation of MB dyes. Wu *et al*. [22] used a low-temperature molten-salt method for the preparation of rod-like Bi_2S_3 single crystals and investigated the effects of annealing temperature and the dosage of molten salt (KSCN) on the morphology and Hg^0 elimination properties of Bi_2S_3, which showed that Bi_2S_3 single crystals have a better Hg^0 capture ability due to the one-dimensional rod-like structure with sufficient exposed adsorption sites, as well as the higher binding energy of Bi^{3+} species. Jia *et al*. [23] utilized a CTAB-assisted hydrothermal synthesis route to obtain 3D Bi_2S_3 for photocatalytic degradation of RhB. However, for the above-mentioned methods for synthesizing Bi_2S_3, complex and expensive equipment is generally required, or additional surfactants, ligands, or toxic organic solvents are needed [20–26], which are not environmentally friendly. Furthermore, most studies have focused on a single morphology of Bi_2S_3, and the research on the 1D/2D Bi_2S_3 is relatively limited, indicating the need for further exploration. The preparation of Bi_2S_3 using hydrothermal synthesis is a simple, economical, and efficient method in terms of environmental sustainability [27], which contributes to a thorough comprehension of the physicochemical and lattice dynamics properties of Bi_2S_3 nanostructures.

Hexavalent chromium (Cr(VI)), a highly toxic metal pollutant, is derived from electroplating, dyeing, and leather manufacturing. Cr(VI) is carcinogenic and mutagenic to humans, animals, and plants through the enrichment of the food chain, posing a serious threat to human health and the ecological environment. The World Health Organization (WHO) has established the maximum concentration of Cr(VI) in drinking water at 50 ppb [28]. In this work, an attempt was made to synthesize 1D, 2D, and 1D/2D Bi_2S_3 materials using a hydrothermal synthesis route combined with an ion-exchange technique. A homemade $Bi_2(H_2O)_2(SO_4)_2(OH)_2$ precursor was utilized for this purpose. The research focused on the photocatalytic reduction of aqueous Cr(VI) using Bi_2S_3 under visible light. Furthermore, the

photocatalytic activities of different photocatalysts were and analyzed through photoelectric tests. Based on the results obtained, a proposed photocatalytic mechanism for the visible-light photocatalytic reduction of aqueous Cr(VI) by Bi_2S_3 was presented.

2. Materials and Methods

2.1 Chemical Reagents

Chemical reagents $Bi(NO_3)_3 \cdot 5H_2O$, $Na_2S \cdot 9H_2O$, sulfuric acid, and anhydrous ethanol were analytically pure and purchased from China National Pharmaceutical Group Chemical Reagent Co.

2.2 Synthesis of Bi_2S_3

$Bi_2(H_2O)_2(SO_4)_2(OH)_2$ precursors were prepared by hydrolysis at room temperature. 10 mmol of $Bi(NO_3)_3 \cdot 5H_2O$ was dissolved in 35 mL of a 10 wt% sulfuric acid solution, was dissolved in 35 mL of 10 wt % sulfuric acid solution, and the hydrolysis reaction was carried out at room temperature with magnetic stirring for 60 min (460 r/min), followed by aging for 120 min. The precipitate was centrifuged, washed to neutrality with deionized water, and dried in an electric draught drying cabinet at 80 °C for 4 h.

Hydrothermal ion-exchange synthesis of precursor Bi_2S_3. 0.5 mmol, 1 mmol, and 2 mmol of homemade $Bi_2(H_2O)_2(SO_4)_2(OH)_2$ were dissolved in 20 mL of deionized water, respectively, and stirred magnetically until well-dispersed. Then three equal parts of 6 mmol $Na_2S \cdot 9H_2O$ were dissolved in 20 mL of deionized water, respectively. Under the condition of continuous stirring, the Na_2S aqueous solution was added drop by drop into a container of $Bi_2(H_2O)_2(SO_4)_2(OH)_2$, and after continued stirring for 30 min, the above solution was sealed in a stainless steel reactor and heated in a blower heating chamber at 190 °C for 24 h. It was naturally cooled to room temperature when the reaction was completed, and the precipitate generated was washed and dried using the above method. The samples were recorded as Bi_2S_3-A, Bi_2S_3-B, and Bi_2S_3-C according to the amount of $Bi_2(H_2O)_2(SO_4)_2(OH)_2$ from small to large. The preparation schematic diagram of 1D/2D Bi_2S_3 is given in Figure 1. Additionally, according to the above procedure for the synthesis of Bi_2S_3, 1 mmol $Bi_2(H_2O)_2(SO_4)_2(OH)_2$ was substituted with 1 mmol $Bi(NO_3)_2 \cdot 5H_2O$ while keeping the other experimental parameters unchanged. The synthesized sample was named Bi_2S_3-D.

2.3 Instrumentation Techniques

The compositional characterization of the synthesized samples was carried out using Bruker AXS D8 ADVANCE X-ray powder diffractometer (XRD, operating voltage 40 kV, operating current 40 mA). The morphology of the synthesized samples was observed using a Hitachi SU8600 scanning electron microscope (SEM, the accelerating voltage was 15 kV). The UV-vis diffuse reflectance spectrum (UV-vis DRS) was obtained by using a PELambda 750UV-vis spectrophotometer ($BaSO_4$ as background, and a slit width of 2 nm, wavelength interval of 1 nm). The electrochemical impedance and transient current of the samples were analyzed using the CHZ660E electrochemical workstation. In the analysis, the platinum sheet served as the auxiliary electrode, the silver chloride electrode was the reference electrode, and the working electrode was the electrode of the photocatalyst fixed on the conductive glass, and the 200 W Xe lamp was used as the light source.

2.4 Photocatalytic Activity Evaluation

The photocatalytic activity of Bi_2S_3 was evaluated by Cr(VI) reduction. 300 mL of 50 mg/L Cr(VI) solution as a simulated pollutant,

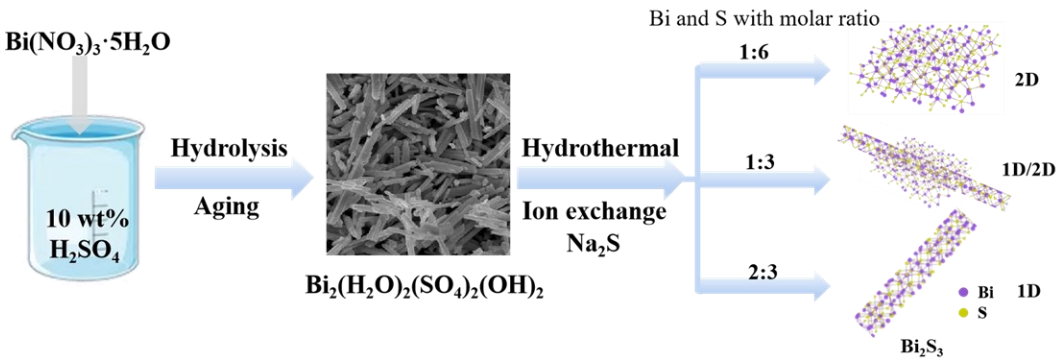

Figure 1. The schematic diagram for the synthesis steps of 1D/2D Bi_2S_3.

which was prepared directly using deionized water. The experimental processes were as follows: 300 mg of the prepared Bi_2S_3 powder was added to the Cr(VI) solution, and the adsorption was first carried out for 100 min under light protection to maintain the adsorption-desorption equilibrium. After the 200 W Xe lamp was turned on (UV light with a λ < 420 nm was filtered out with a light filter), at a fixed time interval of 20 min, about 3.5 mL of the aqueous suspension was fetched from the reactor. Cellulose acetate membranes with a 0.22 μm pore diameter were employed to filter and separate the fetched suspension for removal of the Bi_2S_3. The concentration of Cr(VI) in the filtrate was measured using the diphenylcarbazide spectrophotometry at a wavelength of maximum absorption (λ_{max}) of 542 nm.

The photoreduction rate (R_t) of Cr(VI) solution was calculated using Equation (1), where c_0 and c_t are the concentrations of aqueous Cr(VI) before and after the reaction, respectively.

$$R_t = (c_0\text{-}c_t)/c_0 \times 100\% \quad (1)$$

2.5 Experiments of Active Species Capture in Photocatalytic Reactions

Photocatalytic active species capture experiments were used to analyze and determine the mechanism of visible-light photocatalytic reduction of aqueous Cr(VI) by Bi_2S_3-B. In the experimental operation of 2.3, ·OH was captured by adding 1 mL of 0.4 mol/L isopropanol (IPA), 1 mL of 0.28 mol/L ammonium oxalate solution (AO) for h^+, and 1 mL of 0.06 mol/L p-benzoquinone (BQ) solution for $\cdot O_2^-$, respectively.

3. Results and Discussion

3.1 Structure and Composition

Figure 2 depicts the XRD patterns of synthesized Bi_2S_3 and $Bi_2(H_2O)_2(SO_4)_2(OH)_2$. Comparison with JCPDS card no. 76-1103 shows that the precursor prepared by room temperature hydrolysis is monoclinic phase $Bi_2(H_2O)_2(SO_4)_2(OH)_2$ and no other impurity peaks were detected. By controlling the molar ratios of $Bi_2(H_2O)_2(SO_4)_2(OH)_2$ precursor to sodium sulfide as 1:6, 1:3, and 2:3, Bi_2S_3-A, Bi_2S_3-B and Bi_2S_3-C obtained by hydrothermal synthesis of the precursors had similar XRD diffraction peaks but with differences in the peak intensities. Bi_2S_3-D obtained by direct hydrothermal synthesis also has the same diffraction peak. The overall diffraction peaks presented by the Bi_2S_3 correspond to the orthorhombic phases of Bi_2S_3 (JCPDS card no. 43-1471) with the lattice constant values of a = 11.20 Å, b=11.34 Å, and c=3.99 Å, and no other impurity peaks appeared. The diffraction peaks were located at 2θ values of 15.7°, 17.6°, 22.4°, 23.8°, 24.9°, 28.6°, 31.8°, 35.6°, 39.9°, 46.6°, and 52.6°, which were attributed to the (020), (120), (220), (101), (130), (121), (221), (240), (141), (431), and (132) planes of the Bi_2S_3, respectively. The sharp and intense peaks indicate that pure Bi_2S_3 was prepared with high crystallinity.

The average crystallite size (D) of Bi_2S_3 and $Bi_2(H_2O)_2(SO_4)_2(OH)_2$ were determined using the Debye-Scherrer formula (Equation (2)) [21], where D represents the crystallite size (nm), λ is the wavelength of X-ray radiation (0.15406 nm), K is Scherrer's constant (0.89), β is the full width half maximum, and θ is the diffraction angle.

$$D = K\lambda / (\beta \cos \theta) \quad (2)$$

The average crystallite size of the $Bi_2(H_2O)_2(SO_4)_2(OH)_2$ precursor was 52 nm based on the (120) lattice plane. On the other hand, according to the (130) lattice plane of Bi_2S_3, the average crystallite particle sizes were measured to be 31.13 nm, 34.48 nm, 33.74 nm, and 34.15 nm for Bi_2S_3-A, Bi_2S_3-B, Bi_2S_3-C, and Bi_2S_3-D, respectively.

The nanostructures of synthesized samples were analyzed by SEM to find the influence of the molar ratios of elemental Bi to S in the reaction reagents. Figure 3(a) displays a rod-like morphology of the $Bi_2(H_2O)_2(SO_4)_2(OH)_2$ precursor with length and diameter of 2.58 μm and 0.44 μm, and the surface appears relatively

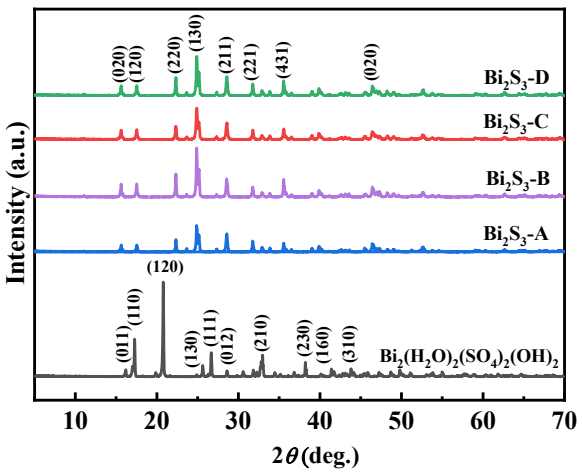

Figure 2. XRD patterns of the synthesized Bi_2S_3-A, Bi_2S_3-B, Bi_2S_3-C, Bi_2S_3-D, and $Bi_2(H_2O)_2(SO_4)_2(OH)_2$ precursor.

rough with a disordered distribution. In Figure 3(b), numerous 2D nanosheet morphologies can be observed, corresponding to Bi_2S_3-A with length and breadth of 0.5 µm and 0.21 µm. Figure 3(c) shows the image of Bi_2S_3-B, exhibiting a 1D/2D heterostructure formed by one-dimensional rods with length and diameter of 0.78 µm and 0.09 µm and two-dimensional sheets with 0.59 µm and 0.23 µm. Both Bi_2S_3-C (Figure 3(d)) and Bi_2S_3-D (Figure 3(d)) prepared from the same molar ratio of Bi to S element, show a rod-like morphology. However, it is still distinguishable that Bi_2S_3-C synthesized from the precursor exhibits a higher (Figure 3(d)) level of rod-like dispersion, with length and diameter of 1.57 µm and 0.11 µm. On the other hand, the rods of Bi_2S_3-D obtained from the direct hydrothermal synthesis of bismuth nitrate, are connected in the form of a "bamboo row" (Figure 3(e)), with length and diameter of 3.41 µm and 0.31 µm, indicating a decrease in the number of reactive active sites exposed on the surface of the photocatalyst. Bi_2S_3 synthesized using hydrothermal synthesis demonstrates a transition from 2D flakes to 1D rods as the Bi^{3+}/S^{2-} molar ratio increased. Figure 2(f) shows the size distribution of the synthesized samples.

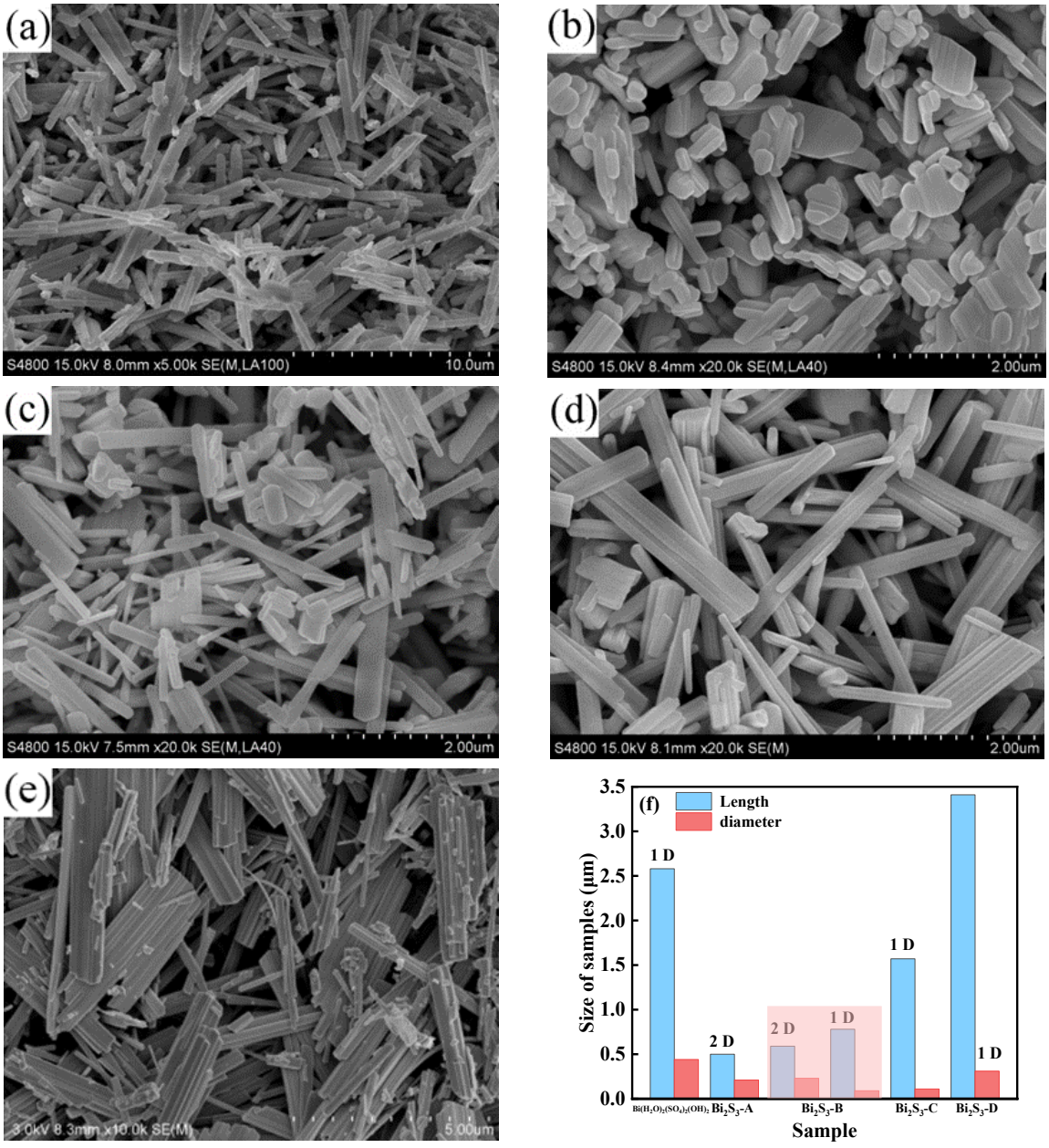

Figure 3. SEM images of (a) $Bi_2(H_2O)_2(SO_4)_2(OH)_2$ precursor, (b) Bi_2S_3-A, (c) Bi_2S_3-B, (d) Bi_2S_3-C, (e) Bi_2S_3-D, and (f) size distribution of synthesized samples.

3.2 Performance of the Synthesized Products in Visible-light Photocatalytic Reduction of Aqueous Cr(VI)

The photocatalytic activity of the photocatalyst depends on the band gap structure. Figure 4(a) shows the UV-vis diffuse absorption spectrum of Bi_2S_3-B. It can be observed in Figure 4(a) that Bi_2S_3-B exhibits significant absorption of visible light between 400 nm and 700 nm. The band gap energy (E_g) of Bi_2S_3-B can be estimated from the Kubelka-Munk function in Equation (3) [29,30]:

$$ahv = B(hv - E_g)^{n/2} \quad (3)$$

where, a represents the light absorption coefficient, h, v, B, and E_g are the Planck constant, light frequency, an energy-independent constant, and the band gap of a semiconductor material, respectively. The value of n depends on the optical transition characteristics of the semiconductor, with n being 1 for the direct transition and 4 for the indirect transition. Bi_2S_3 is a direct band gap semiconductor [29,30]. By plotting $(ahv)^2$ versus hv can exhibit the calculated E_g of Bi_2S_3-B is 1.33 eV. Furthermore, the valence band potential of Bi_2S_3 was estimated to be 1.425 eV using Equation (4) [31], which is consistent with previous reports [16,32]. Therefore, the conduction band (CB) potential of Bi_2S_3 was further estimated to be 0.095 eV according to the formula of $E_{CB} = E_{VB} - E_g$.

$$E_{VB} = X - E_e + 0.5E_g \quad (4)$$

The visible-light photocatalytic performance of synthesized Bi_2S_3 was carried out with 50 mg/L aqueous Cr(VI) as a target contaminant as shown in Figure 5. The adsorption experiments of Bi_2S_3 on Cr(VI) solution revealed that the concentration of Cr(VI) remained constant after 100 minutes, indicating the adsorption-desorption equilibrium was reached. Upon visible light irradiation, the concentration of Cr(VI) in different photocatalyst systems decreases further with increasing light exposure time. After 140 minutes of visible-light irradiation, the reduction of Cr(VI) by Bi_2S_3-A, Bi_2S_3-B, Bi_2S_3-C and Bi_2S_3-D was 51.0%, 54.5%, 34.9% and 40.5%, respectively. The synthesized Bi_2S_3 exhibits significant photocatalytic activity in reducing Cr(VI) under visible light. The fabricated Bi_2S_3-A has a 2D sheet structure, but the lamination phenomenon occurs due to the high surface energy of the nanosheets, which covers part of the reactive active sites on the surface of the photocatalyst and hinders the transmission of the photogenerated carriers. In contrast, Bi_2S_3-B has a 1D/2D heterogeneous structure, which reduces the coverage of the active sites and can improve the separation and transmission of photogenerated carriers. Therefore, the photocata-

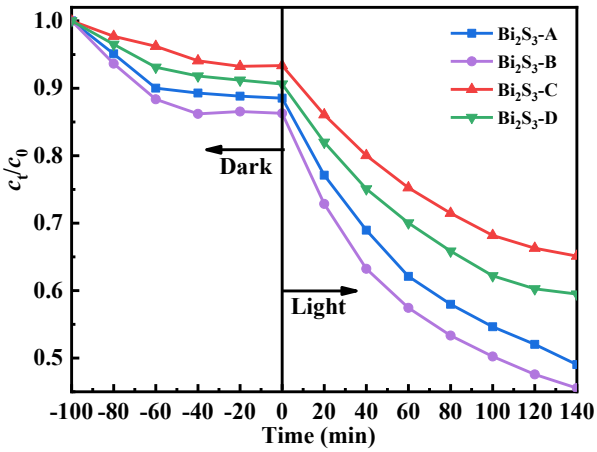

Figure 5. Performance of Bi_2S_3-A, Bi_2S_3-B, Bi_2S_3-C, and Bi_2S_3-D in the adsorption and visible-light-induced photocatalytic reduction of aqueous Cr(VI).

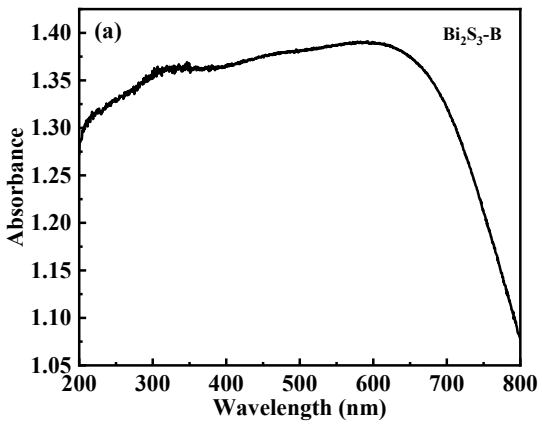

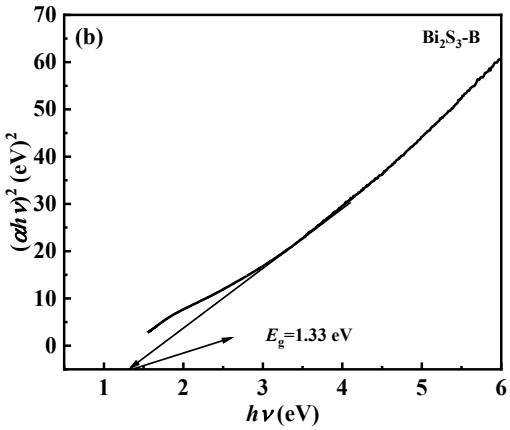

Figure 4. (a) UV-vis diffuse reflection spectra; and (b) Tauc plots of Bi_2S_3-B.

lytic activity of Bi_2S_3-B is higher than that of Bi_2S_3-A. Subsequently, the photocurrent and electrochemical impedance spectroscopy were used to further verify the production and separation of photogenerated charge carriers on the photocatalyst.

The reaction rate constants (k) for the photocatalytic reduction of Cr(VI) by Bi_2S_3 were calculated using the pseudo-first kinetic equation (5) [32–34], where c_t and c_0 represent the concentration of aqueous Cr(VI) at time t and 0 min, respectively:

$$\ln (c_0/c_t) = k\, t \qquad (5)$$

The higher activity of Bi_2S_3-B, synthesized using the precursor method, can be attributed to its 1D rod-like and 2D nanosheet structures, which provide more reactive active sites. Additionally, the unique 1D/2D heterostructure facilitates the transport and transfer of photogenerated carriers. According to the $\ln(c_0/c_t)$ against t (Figure 6)) plots, the k values for the systems containing Bi_2S_3-A, Bi_2S_3-B, Bi_2S_3-C, and Bi_2S_3-D were determined to be 0.0054, 0.0064, 0.0036, and 0.0042 min^{-1}, respectively. The Bi_2S_3-B with a 1D/2D morphology, synthesized as a precursor, exhibits the highest efficiency in the photocatalytic reduction of Cr(VI). The experimental results indicate that the 1D rod-like and 2D nanosheet structure of Bi_2S_3-B allows for more reactive active sites. In particular, the unique 1D/2D heterostructure is favorable for the transport and transfer of photogenerated carriers.

3.3. Photocatalytic Mechanism of Bi_2S_3-B

To experimentally verify the higher transfer and separation efficiency of photogenerated carriers in Bi_2S_3-B, both electrochemical impedance spectra and transient photocurrent response measurements were conducted. Figure 7(a) illustrates the electrochemical impedance spectra, demonstrating that the Nyquist arc radius follows the order of Bi_2S_3-B > Bi_2S_3-A > Bi_2S_3-D > Bi_2S_3-C. Since the arc radius of the Nyquist arc radius is directly proportional to the charge transfer resistance [35–37], the smallest Nyquist arc radius of Bi_2S_3-B indicates a faster charge transfer rate. Furthermore, the transient photocurrent response of Bi_2S_3 was assessed, as displayed in Figure 7(b) Bi_2S_3-B exhibited a larger photocurrent, indicating that Bi_2S_3-B is more proficient in generating and separating h^+ and e^- [35–37]. Additionally, the greater decline in the photoresponse after turning off the light indicates that the photogenerated carriers exist for a shorter duration and are prone to recombination on the surface or interior of the photocatalyst.

To elucidate the reaction mechanism of the photocatalytic reduction of Cr(VI) by Bi_2S_3-B, free radical trapping experiments were conducted to detect the active species present in the photocatalytic system. Various trapping

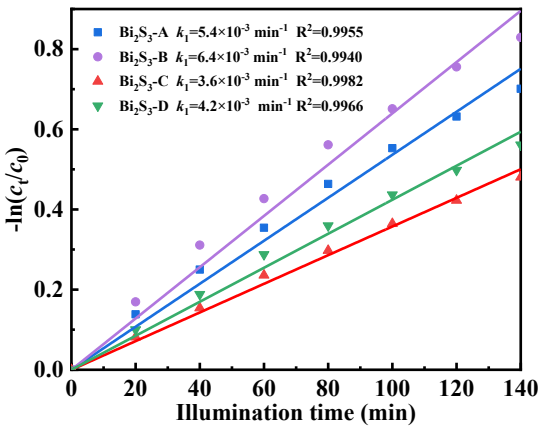

Figure 6. Determination of k values of Bi_2S_3-A, Bi_2S_3-B, Bi_2S_3-C, and Bi_2S_3-D using the plots of ln (C_0/C_t) vs. t.

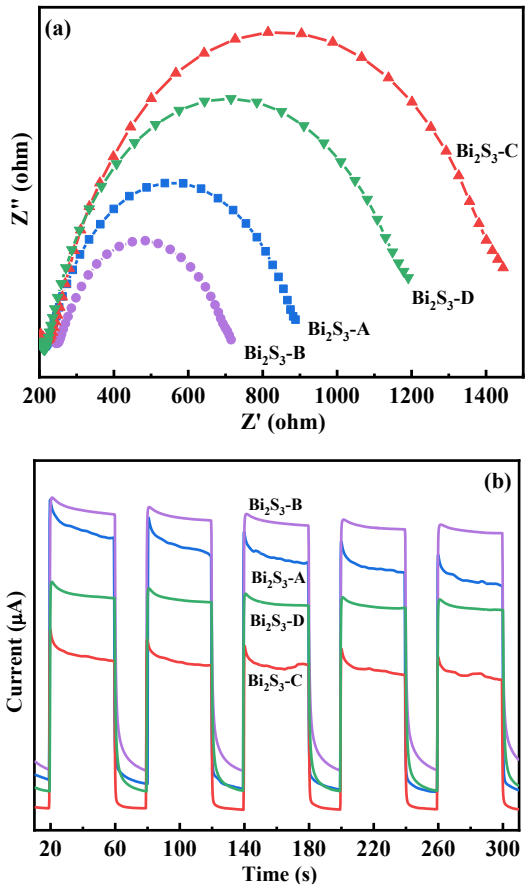

Figure 7. (a) Electrochemical impedance spectra, and (b) transient photocurrent response spectra of Bi_2S_3-A, Bi_2S_3-B, Bi_2S_3-C and Bi_2S_3-D.

agents, including BQ, AO, and IPA were utilized to capture $\cdot O_2^-$, h^+, and $\cdot OH$, respectively, as depicted in Figure 8. The results revealed that the photoreduction efficiency of Cr(VI) decreased to 28.7% and 43.1% upon the addition of AO and BQ, respectively. However, the addition of quantitative IPA had minimal impact effect on the photocatalytic reduction rate of Cr(VI). The experimental findings suggested that $\cdot O_2^-$ and h^+ were the predominant active species involved in the photocatalytic process.

According to the aforementioned experimental results, the photocatalytic reduction mechanism of Cr(VI) by Bi_2S_3-B can be described in Figure 9. Specifically, When Bi_2S_3-B is exposed to visible light irradiation, it absorbs photon energy, leading to the generation of h^+ and e^-. The conduction band holes of Bi_2S_3-B oxidize water, resulting in the production of O_2, which then combines with e^- to form $\cdot O_2^-$, consequently reducing Cr(VI) to Cr(III). Moreover, the photogenerated electrons in the conduction band of Bi_2S_3-B can directly participate in the reduction of Cr(VI) to Cr(III). Overall, the process can be represented by the following reaction equations:

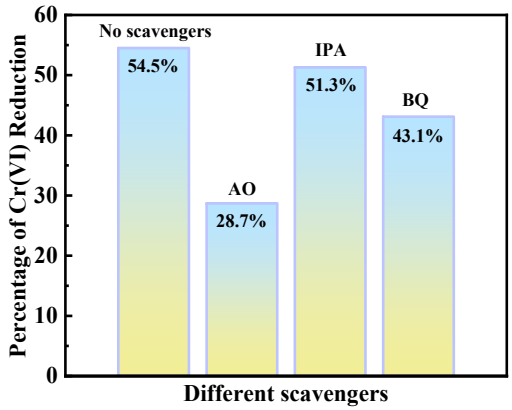

Figure 8. Trapping experiment for photoreduction of aqueous Cr(VI) over Bi_2S_3-B photocatalyst (BQ for $\cdot O_2^-$, AO for h^+ and IPA for $\cdot OH$).

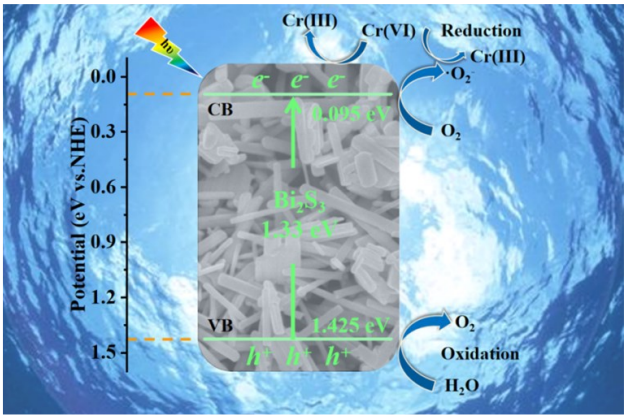

Figure 9. Photocatalytic reduction mechanism of Cr(VI) by Bi_2S_3.

$$Bi_2S_3 + h\nu \rightarrow Bi_2S_3\ (e^-) + Bi_2S_3\ (h^+) \quad (6)$$
$$Bi_2S_3\ (h^+) + H_2O \rightarrow O_2 \quad (7)$$
$$Bi_2S_3\ (e^-) + O_2 \rightarrow \cdot O_2^- \quad (8)$$
$$\cdot O_2^- + Cr(VI) \rightarrow Cr(III) + O_2 \quad (9)$$
$$e^- + Cr(VI) \rightarrow Cr(III) \quad (10)$$

4. Conclusions

The synthesis of orthorhombic Bi_2S_3 photocatalysts with a 1D/2D heterogeneous morphology structure was successfully achieved through a simple hydrothermal method, utilizing homemade $Bi_2(H_2O)_2(SO_4)_2(OH)_2$ precursors. By adjusting the molar ratio of elemental Bi to S in the reaction reagents, it was possible to synthesize either 2D sheet or 1D rod Bi_2S_3 structures. Among the different synthesized morphologies, the Bi_2S_3 with a 1D/2D heterogeneous structure exhibited the highest photocatalytic activity in the reduction of aqueous Cr(VI), along with the fastest photogenerated carrier mobility and the lowest recombination rate. This superior performance can be attributed to the unique combination of 1D and 2D morphologies, facilitating efficient separation of photogenerated carriers and minimizing recombination. The findings of this study have significant implications in the field of energy conversion and environmental treatment. The ability to modulate the morphology of photocatalysts with a 1D/2D heterogeneous structure presents new opportunities for enhancing their photocatalytic activity and efficiency, ultimately contributing to the development of more effective and sustainable photocatalytic systems for the reduction of Cr(VI) in water.

Acknowledgments

This research was financially supported by the Science and Technology Project of Xuzhou (NO. KC21286), the Natural Science Foundation of China (NO. 22202169), Innovation and entrepreneurship projects for college students (xcx2023007, xcx2023018).

CRediT Author Statement

Xinzhuo Wu and *Shaojie Chen*: Investigation, Original draft & writing. *Yinxing Jiang* and *Xinshan Zhao*: Formal analysis, Investigation. *Zhao Li*: Revision, Funding. *Yingmei Zhou*: Review, Editing. *Jing Li*: Super vision, Design, Revision & Funding.

References

[1] Nawaz, A., Goudarzi, S., Asghari, M. A., Pichiah, S., Selopal, G.S., Rosei, F., Wang, Z.M., Zarrin, H. (2021). Review of hybrid 1D/2D photocatalysts for light-harvesting applications. *ACS Applied Nano Materials*, 4 (11), 11323-11352. DOI: 10.1021/acsanm.1c01014.

[2] Hou, H., Zhang, X. (2020). Rational design of 1D/2D heterostructured photocatalyst for energy and environmental applications. *Chemical Engineering Journal*, 395, 125030. DOI: 10.1016/j.cej.2020.125030.

[3] Kadem, A.J., Tan, Z.M., Suntharam, N.M., Pung, S., Ramakrishnan, S. (2023). Synthesis of CuO, ZnO and SnO_2 Coupled TiO_2 photocatalyst particles for enhanced photodegradation of rhodamine B dye. *Bulletin of Chemical Reaction Engineering & Catalysis*, 18 (3), 506-520. DOI: 10.9767/bcrec.19532.

[4] Qian, H., Wang, B., Liu, M., Zhao, N., Wang, Z., Peng, Y. (2021). Unique 1D/2D $Bi_2O_2CO_3$ nanorod-Bi_2WO_6 nanosheet heterostructure: synthesis and photocatalytic performance. *CrystEngComm*, 23 (35), 6128-6136. DOI: 10.1016/j.solidstatesciences.2017.07.003.

[5] Li, J., Wu, C., Dong, B., Li, J., Zhao, L., Wang, S. (2022). 1D/2D TiO_2/$ZnIn_2S_4$ S-scheme heterojunction photocatalyst for efficient hydrogen evolution. *Chinese Journal of Catalysis*, 42 (2), 339-349. DOI: 10.1016/s1872-2067(21)63875-5.

[6] Jiang, M., Xu, J., Munroe, P., Xie, Z. (2023). 1D/2D CdS/WS_2 heterojunction photocatalyst: first-principles insights for hydrogen production, *Materials Today Communications*, 35, 105991. DOI: 10.1016/j.mtcomm.2023.105991.

[7] Gong, H., Zhao, C., Niu, G., Zhang, W., Wang, F. (2020). Construction of 1D/2D α-Fe_2O_3/SnO_2 Hybrid Nanoarrays for Sub-ppm Acetone Detection, *Research*. DOI: 10.34133/2020/2196063.

[8] Zhu, Z., Xia, H., Li, X., Li, H. (2023). A novel 1D/2D rod-sheet shape $Cu_3Mo_2O_9$/g-C_3N_4 heterojunction photocatalyst with enhanced photocatalytic performance for ciprofloxacin, *Optical Materials*, 136, 113420. DOI: 10.1016/j.optmat.2022.113420.

[9] Li, Y., Wang, L., Cai, T., Zhang, S., Liu, Y., Song, Y., Dong, X., Hu, L. (2017). Glucose-assisted synthesize 1D/2D nearly vertical CdS/MoS_2 heterostructures for efficient photocatalytic hydrogen evolution, *Chemical Engineering Journal*, 321, 366-374. DOI: 10.1016/j.cej.2017.03.139.

[10] Wang, X., Ren, Y., Li, Y., Zhang, G. (2021). Fabrication of 1D/2D $BiPO_4$/g-C_3N_4 heterostructured photocatalyst with enhanced photocatalytic efficiency for NO removal, *Chemosphere*, 287, 132098. DOI: 10.1016/j.chemosphere.2021.132098.

[11] Li, Y., Huang, L., Li, B., Wang, X., Zhou, Z., Li, J., Wei, Z. (2016). Co-nucleus 1D/2D Heterostructures with Bi_2S_3 Nanowire and MoS_2 Monolayer: One-Step Growth and Defect-Induced Formation Mechanism, *ACS Nano*, 10 (9), 8938-8946. DOI: 10.1021/acsnano.6b04952.

[12] Vattikuti, S.P., Shim, J., Byon, C. (2018). 1D Bi_2S_3 nanorod/2D e-WS_2 nanosheet heterojunction photocatalyst for enhanced photocatalytic activity, *Journal of Solid State Chemistry*, 258, 526-535. DOI: 10.1016/j.jssc.2017.11.017.

[13] Wang, X., Zhang, H., Wang, W., Zhang, G., Chu, X., Cao, J. (2022). Synthesis of 1D/2D Bi_2S_3@Ti_3C_2 heterojunction with superior photocatalytic removal ability of tetracycline hydrochloride, *Materials Letters*, 326, 132907. DOI: 10.1016/j.matlet.2022.132907.

[14] Motaung, M.P., Onwudiwe, D.C., Lei, W. (2021). Microwave-assisted synthesis of Bi_2S_3 and Sb_2S_3 nanoparticles and their photoelectrochemical properties, *ACS Omega*, 6 (29), 18975-18987. DOI: 10.1021/acsomega.1c02249.

[15] Kashmery, H.A., EI-Hout, S.I. (2023). Bi_2S_3/Bi_2O_3 nanocomposites as effective photocatalysts for photocatalytic degradation of tetracycline under visible-light exposure, *Optical Materials*, 135, 113231. DOI: 10.1016/j.optmat.2022.113231.

[16] Helal, A., Harraz, F.A., Ismail, A.A., Sami, T.M., Ibrahim, I.A. (2017). Hydrothermal synthesis of novel heterostructured Fe_2O_3/Bi_2S_3 nanorods with enhanced photocatalytic activity under visible light, *Applied Catalysis B: Environmental*, 213, 18-27. DOI: 10.1016/j.apcatb.2017.05.009.

[17] Zhang, R., Li, Y., Zhang, W., Sheng, Y., Wang, M., Liu, J., Liu, Y., Zhao, C., Zeng, K. (2021). Fabrication of Cu_2O/Bi_2S_3 heterojunction photocatalysts with enhanced visible light photocatalytic mechanism and degradation pathways of tetracycline, *Journal of Molecular Structure*, 1229, 129581. DOI: 10.1016/j.molstruc.2020.129581.

[18] Helal, A., Harraz, F.A., Ismail, A.A. (2021). One-step synthesis of heterojunction Cr_2O_3 nanoparticles decorated Bi_2S_3 nanorods with enhanced photocatalytic activity for mineralization of organic pollutants, *Journal of Photochemistry and Photobiology A: Chemistry*, 419, 113468. DOI: 10.1016/j.jphotochem.2021.113468.

[19] Li, X., Jun, L., Xiao, J., Xu, Y., Yang, C., Tang, J., Zhao, K., Gong, X., Zhou, X., Zou, H. (2022). Study on the relationship between Bi_2S_3 with different morphologies and its photocatalytic hydrogen production performance, *Journal of Analytical Science and Technology*, 13 (1), 1-8. DOI: 10.1186/s40543-022-00325-6.

[20] Arumugam, J., George, A., Venci, X., Raj, A.D., Irudayaraj, A.A., Josphine, R.L., Sundaram, S.J., Al-onazi, W.A., Al-Mohaimeed, A.M., Chen, T.W., Kaviyarasu, K. (2022). Exploring and fine tuning the properties of one dimensional Bi_2S_3 nanorods, *Journal of Alloys and Compounds*, 902, 163785. DOI: 10.1016/j.jallcom.2022.163785.

[21] Sasikala, S., Balakrishnan, M., Kumar, M., Chang, J.H. (2023). Effect of solvent mixtures on the unique morphology for photocatalytic activity of Bi_2S_3 nanoparticles synthesized by microwave irradiation method, *Inorganic Chemistry Communications*, 153, 110854. DOI: 10.1016/j.inoche.2023.110854.

[22] Wu, J., Yang, L., Jia, T., Liu, D. (2022). Salt-assisted synthesis of rod-like Bi_2S_3 single crystals for gas-phase elemental mercury removal, *Energy & Fuels*, 36 (5), 2591-2599. DOI: 10.1021/acs.energyfuels.1c04286.

[23] Jia, T., Wang, X., Long, F., Li, J., Kang, Z., Fu, F., Sun, G., Chen, J. (2016). Facile synthesis, characterization, and visible-light photocatalytic activities of 3D hierarchical Bi_2S_3 architectures assembled by nanoplatelets, *Crystals*, 6 (11), 140. DOI: 10.3390/cryst6110140.

[24] Lee, S., Kim, M.S., Lee, H., Lee, S.Y. (2022). Organic bromide-assisted one-pot synthesis of Bi_2S_3 nanorods using DMSO as a sulfur supply, *CrystEngComm*, 24 (26), 4713-4722. DOI: 10.1039/d2ce00568a.

[25] Arumugam, J., Raj, A.D., Irudayaraj, A.A., Thambidurai, M. (2018). Solvothermal synthesis of Bi_2S_3 nanoparticles and nanorods towards solar cell application, *Materials Letters*, 220, 28-31. DOI: 10.1016/j.matlet.2018.02.123.

[26] Jiang, Y., Zhu, Y., Xu, Z. (2006). Rapid synthesis of Bi_2S_3 nanocrystals with different morphologies by microwave heating, *Materials Letter*s, 60 (17-18), 2294-2298. DOI: 10.1016/j.matlet.2005.12.127.

[27] Do, T., Vu, T., Ho, G., Pham, Q., Giang, H., Le, A., Tran, D. (2021). Bi_2S_3 nanowires: first-principles phonon dynamics and their photocatalytic environmental remediation, *The Journal of Physical Chemistry C*, 125 (7), 4086-4091. DOI: 10.1021/acs.jpcc.0c10849.

[28] Wang, C., Liu, N., Zhao, X., Tian, Y., Chen, X., Zhang, Y., Fan, L., Hou, B. (2023). C-doped BiOCl/Bi_2S_3 heterojunction for highly efficient photoelectrochemical detection and photocatalytic reduction of Cr(VI), *Journal of Materials Science & Technology*. DOI: 10.1016/j.jmst.2023.03.066.

[29] Wang, F., Liu, Z., Dong, Y., Sun, H. (2022). Boosting visible light photocatalysis of $Ag_6Si_2O_7$/dandelion shaped Bi_2S_3 heterojunctions, *Colloids and Surfaces A: Physicochemical and Engineering*, 643, 128732. DOI: 10.1016/j.colsurfa.2022.128732.

[30] Lan, M., Wang, Y., Dong, X., Yang, F., Zheng, N., Wang, Y., Ma, H., Zheng, X. (2022). Controllable fabrication of sulfur-vacancy-rich Bi_2S_3 nanorods with efficient near-infrared light photocatalytic for nitrogen fixation, *Applied Surface Scienc*e, 591, 153205. DOI: 10.1016/j.apsusc.2022.153205.

[31] Shen, S., Li, X., Zhou, Y., Han, L., Xie, Y., Deng, F., Huang, J., Chen, Z., Feng, Z., Xu, J., Dong, F. (2023). Novel BiOBr/Bi_2S_3 high-low junction prepared by molten salt method for boosting photocatalytic degradation and H_2O_2 production, *Journal of Materials Science & Technology*, 155, 148-159. DOI: 10.1016/j.jmst.2023.03.006.

[32] Zhao, G., Zheng, Y., He, Z., Lu, Z., Wang, L., Li, C., Jiao, F., Deng, C. (2018). Synthesis of Bi_2S_3 microsphere and its efficient photocatalytic activity under visible-light irradiation, *Trans. Nonferrous Met. Soc.*, 28, 2002−2010. DOI: 10.1016/S1003-6326(18)64844-7.

[33] Iqbal, M., Ibrar, A., Ali, A., Hussain, S., Shada, S., Ullah, S., Alshahrani, T., Hakami, J., Khan, F., Thebo, K.H. (2022). Facile Synthesis of Mn doped Bi_2S_3 Photocatalyst for Efficien egradation of Organic Dye under Visible-Light Irradiation, *Journal of Molecular Structure*, 1267, 133598. DOI: 10.1016/j.molstruc.2022.133598

[34] Liang, P., Yuan, L., Du, K., Wang, L., Li, Z., Deng, H., Wang, X., Luo, S., Shi, W. (2021). Photocatalytic reduction of Uranium(VI) under visible light with 2D/1D Ti_3C_2/CdS, *Chemical Engineering Journal*, 420, 129831. DOI: 10.1016/j.cej.2021.129831.

[35] Jiang, M., Shi, Y., Huang, J., Wang, L., She, H., Tong, J., Su, B., Wang, Q. (2018). Synthesis of Flowerlike g-C_3N_4/BiOBr with Enhanced Visible Light Photocatalytic Activity for Dye Degradation, *Eur. J. Inorg. Chem.*, 1834–1841. DOI: 10.1002/ejic.201800110.

[36] Huang, L., Liu, J., Li, P., Li, Y., Wang, C., Shu, S., Song, Y. (2022). CQDs modulating Z-scheme g-C_3N_4/BiOBr heterostructure for photocatalytic removing RhB, BPA and TC and E. coli by LED light, *Journal of Alloys and Compounds*, 895, 162637. DOI: 10.1016/j.jallcom.2021.162637.

[37] Wu, Y., Han, Q., Wang, L., Wang, X., Zhu, J. (2017). One-pot synthesis of 3D hierarchical Bi_2S_3/$(BiO)_2CO_3$ hollow microspheres at room temperature and their photocatalytic performance, *Materials Chemistry and Physics*, 187, 72-81. DOI: 10.1016/j.matchemphys.2016.11.049.